KSME

Springer

Journal of Mechanical Science and Technology 37 (10) 2023

Original Article
DOI 10.1007/s12206-023-0901-z

Keywords:
· Profile optimization
· Turnouts
· Wheel-rail contact
· Rolling radius difference function
· Wheel profile

Correspondence to:
Dilai Chen
chendilai@163.com

Citation:
Chen, D., Sun, G., Xing, L., Wu, Y., Shen, G. (2023). A grinding profile design method for rails in the switch area considering a representative set of wheel profiles. Journal of Mechanical Science and Technology 37 (10) (2023) 4923~4933. http://doi.org/10.1007/s12206-023-0901-z

Received May 17th, 2022
Revised June 19th, 2023
Accepted July 4th, 2023

† Recommended by Editor
No-cheol Park

A grinding profile design method for rails in the switch area considering a representative set of wheel profiles

Dilai Chen[1], Gengchen Sun[1], Li Xing[1], Yubo Wu[1] and Gang Shen[2]

[1]School of Railway Transportation, Shanghai Institute of Technology, Shanghai, China, [2]Railway and Urban Rail Transit Research Institute, Tongji University, Shanghai, China

Abstract This study introduces an inverse rail profile design method for rails in the switch area of railway turnouts, which allows one to improve the wheel-rail contact and dynamic performance of rail vehicles during their passage of turnouts. Given the structure of rails in turnouts, this method employs the rolling radius difference function for the primary design basis, which is also the primary objective function. Using the expected distribution law between wheels and rails as a boundary condition, the Euler method is adopted to solve the differential equation for the rail ordinate under optimization based on given the transverse coordinates of rail. The robustness of the test is realized by optimizing the rail profiles for a representative set of wheel profiles. After the optimization, rail and wheel profiles are better matched, which improves the dynamic performance of rail vehicles crossing turnouts. This optimization method is quite efficient, and its results are reasonable.

1. Introduction

To guide rail vehicles from one track to another at a railway junction, turnouts are used worldwide as integral components of railway infrastructure. Insofar as the design of turnouts implies a rail geometry discontinuity in the switch area, high impact loads and larger lateral displacements (or even flange contact) occur when rail vehicles cross the switch areas. These factors intensified the wear processes between wheels and rails and cause rail rolling contact fatigue. Therefore, rails in switch areas are more susceptible to damage (such as surface cracking and crumbling, shelling, excessive wear, plastic deformations, general fracture, etc.), which implies a higher maintenance cost [1-3]. As an essential approach of railway maintenance, rail grinding technology can eliminate and inhibit rail surface damage and, thus, prolong the rail surface life [4].

In rail operations, the dynamic wheel-rail interaction, rail wear, and train operation safety are closely related to the wheel-rail geometric matching. The reasonable improvement of the wheel-rail contact enhances the train operation safety and dynamic performance, reduces the wheel-rail wear, and effectively prolongs the service life of rails [5]. Shevtsov et al. [6, 7], proposed a wheel tread design optimization method based on rolling radius difference function (RRDF) and employed the numerical analysis method to optimize the wheel tread design, which improved the vehicle operation performance and reduced the wheel-rail contact wear. This approach implied a multipoint approximation based on responsive surface fitting to design an optimum wheel profile that matched a target RRD, as well as accounted for the rolling contact fatigue and wear. Shen et al. [8] adopted RRDF as the design goal to inversely derive the wheel tread of rail vehicles, which resulted in the reduced wheel-rail contact stress and more uniform wear distribution. Respective software programs have also been developed. Cui et al. [9] used the wheel-rail normal-direction clearance as a starting point to optimize the wheel tread design, which effectively reduced the wheel-rail contact stress, but the calculation efficiency is low. Ignesti et al. [10] optimized the wheel profile by the minimal wear criterion, which efficiently

alleviated wear and improved the operation stability. Santamaria et al. [11] proposed a wheel tread profile optimization method using the genetic algorithm, with the equivalent conicity curve used as the objective function.

The optimal design of the rail profile is more complicated than the optimal design of the wheel tread. Choi [12] performed the asymmetric profile design of curved rails utilizing the genetic algorithm to improve the vehicle dynamic negotiation performance and alleviate the side grinding-induced wear of rails. Wang et al. [13] proposed a rail design method for heavy-haul railways based on the wheel-rail rolling contact theory and the nonlinear programming theory. Their approach considered the rail variation throughout its service life, and the goal of the design was to minimize the metal wear and grinding throughout the design cycle. Mao et al. [14, 15] introduced an inverse method to derive rail grinding profile using RRDF as the optimization objective function. When this method was applied for the inverse design of rails, the wheel contact point was used as a known condition. As a result, the profile of the designed rail was continuous and linear, which was not suitable for developing the characteristic concave curve shape of rails in the switch area. Zhai et al. [16] proposed an asymmetrical rail profile design method based on the dynamic wheel-rail interaction forces for the problem of serious side grinding of a small-radius curve in heavy-duty railways. The results obtained indicated that the wheel-rail dynamic action was improved while the rail side wear was reduced.

There are few studies on the optimization of turnouts. As the wheel-rail contact relation is more complicated in the turnout area, the profile is variable along the longitudinal direction. In the switch area, when the switch rail is attached to the stock rail, there is a concave space. So that design the rail profiles in the turnout area is greater challenges than that in the interval line. Nicklisch [17] optimized the vertical stiffness of the switch area in turnouts by adjusting the stiffness of the fastener or sleeper, which reduced the dynamic force between wheel and rail. By optimizing the gauge of the switch area, the tangential force of wheel and rail contact could be reduced, thus minimizing the rail wear in the switch area. Wang [18] employed the quadratic sequence method to minimize RRDF and optimize switch rails in the switch area of turnouts, which ensured relatively high vehicle stability when it crossed a turnout straightly at high speed. But this method only optimized a section of the switch area and the calculation efficiency is low. Pålsson [19, 20] proposed the turnout profile is optimized with the objective of contact stress and energy dissipation, but each profile is optimized based on several control points, which requires a higher selection of control points. To account for the additional vertical loads applied to the rails in the switch area, Bugarín [21] proposed to widen the gauge in the switch area of a turnout to optimize the impact load in the turnout area. Oswald [22] using the “kinematic gauge optimization” method to reduce the dynamic force when the wheel turns from the stock rail to the switch rail. The wheel-rail force can be reduced by as much as 50 %. Nielsen [23] aims to reduce contact stress in the turnout area by optimizing the switch panel geometry. Chen [24] designed the radius of rail profile in turnout area based on Hertz contact stress to reduce the contact stress between wheel and rail.

At present, the wheel-rail dynamics, including stability, steering ability, and contact stress distribution, is govern by two functions, namely: (i) the contact angle function (CAF), which is the left and right contact angle difference versus wheelset lateral movement, and (ii) the rolling radius difference function (RRDF), which refers to the left and right rolling radius difference versus wheelset lateral movement. RRDF is one of the primary functions characterizing the contact between the wheelset and rail. It has a significant impact on the vehicle stability, curving performance, as well as the wheel-rail wear. It also determines the dynamic performance of the wheelset [8, 14, 15].

In this paper, using RRDF as the primary design basis, proposes a grinding profile design method for switch rails in turnouts focusing on wheel-rail dynamic performance optimization. Using the expected wheel-rail contact distribution as a boundary condition, the design of the rail ordinate is obtained by directly reversing the known rail abscissa range. The Euler method is used to solve the resulting differential equation. Several sections in the turnout area (switch rail width of 0 mm, switch rail width of 20 mm, switch rail width of 35 mm, switch rail width of 50 mm, full width of switch rail) are very important sections, so only these control sections are optimized [25, 26]. In order to verify the robustness of the design method, a representative set of wheel profiles are selected to verify the optimization results [19].

2. Mathematical modeling

The definitions of wheel-rail coordinate systems are established, according to the right-hand rule (see Fig. 1). The Y-axis of the rail coordinate system (Y_r) is the common tangent line at the top of the rail, with the positive direction pointing to the right. The Z-axis is perpendicular to the Y_r axis, with the positive direction pointing down. When the wheel and rail are in contact, the local rail coordinate system origin O_r coincides with that of the global coordinate system. The Y-axis of the wheelset coordinate system (Y_w) lies along with the axis of the wheelset, with the positive direction pointing to the right. The Z axis (Z_w) is perpendicular to the Y_w axis, with the positive direction pointing

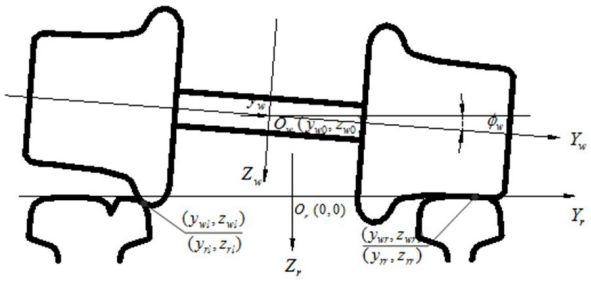

Fig. 1. Schematic of single point contact between the rigid wheel and rail.

down. The origin O_w is located at the mass center of the wheelset. Given any lateral displacement y_w for the wheelset, the center of the wheelset in the global coordinate system is (y_{w0}, z_{w0}). Here z_{w0} is approximated as the rolling wheel radius, and the wheelset has a rolling angle Φ_w. The wheel-rail contact points are given in their corresponding local coordinate systems, such that the left and right contact points are defined as (y_{wl}, z_{wl}) and (y_{wr}, z_{wr}), respectively, in the wheel-set coordinate system and as (y_{rl}, z_{rl}) and (y_{rr}, z_{rr}), respectively, in the rail one.

To simplify the problem and analyze the general patterns, the following assumptions are made:

1) Both wheels and rails are rigid such that their elastic deformations at contact are negligible in comparison to their corresponding external dimensions. In other words, the situation that a lateral displacement value corresponds to multiple rolling radius differences, which will lead to various optimization results should be avoided. The uniqueness of wheel-rail geometrical contact should be ensured.

2) The designed rail profile is a convex curve such that the slope of the tangent line varies monotonically at each point. For the special structure in the turnout area, it is necessary to piecewise optimized designed, and then combine the designed profile.

3) The section abscissa of the designed rail should maintain as monotonic as possible.

4) The rail profile designed by grinding shall not exceed the original profile.

5) The influence of the yaw angle in small range of the wheelset on the rolling radius difference curve is ignored [27].

Since the roll angle of the wheelset (ϕ_w) is very small, we have made the following simplification,

$$\phi_w \approx \sin(\phi_w) \approx \tan(\phi_w), \cos(\phi_w) \approx 1 . \tag{1}$$

According to the wheel rail contact point, it is the same point in the spatial position of wheel and rail profile. Therefore,

$$z_{rl} = y_{wl}\sin\phi_w + z_{wl}\cos\phi_w + z_{w0} \tag{2}$$

$$z_{rr} = y_{wr}\sin\phi_w + z_{wr}\cos\phi_w + z_{w0} . \tag{3}$$

There must be a common normal at the contact point due to the overlap of contact points in space, such that

$$\frac{\mathrm{d}z_{rl}}{\mathrm{d}y_{rl}} = \tan\left(\operatorname{atan}\frac{\mathrm{d}z_{wl}}{\mathrm{d}y_{wl}} + \phi_w\right) \tag{4}$$

$$\frac{\mathrm{d}z_{rr}}{\mathrm{d}y_{rr}} = \tan\left(\operatorname{atan}\frac{\mathrm{d}z_{wr}}{\mathrm{d}y_{wr}} + \phi_w\right) . \tag{5}$$

The geometric relationship between the roll angle and other contact parameters can be written as follows:

$$\tan\phi_w = \frac{z_{wl} - z_{wr} - \dfrac{z_{rl} - z_{rr}}{\cos\phi_w}}{|y_{wr}| + |y_{wl}|} \tag{6}$$

The RRDF curve is defined as:

$$\Delta R = z_{wl} - z_{wr} . \tag{7}$$

Based on assumption Eq. (1), the following equations are valid when there is only one contact point between the wheel and rail in space:

$$z_{wl}(y_w) - z_{wr}(y_w) = \min\{z_{wl}(y_w) - z_{wr}(y_w)\big|_{y=yw}\} \tag{8}$$

$$sign\left(\frac{dz_{wl}}{dy_{wl}}\right) = sign\left(\frac{dz_{rl}}{dy_{rl}}\right) \equiv 1 ; \quad sign\left(\frac{dz_{wr}}{dy_{wr}}\right) = sign\left(\frac{dz_{rr}}{dy_{rr}}\right) \equiv -1 . \tag{9}$$

Based on assumption Eq. (2), the rail is a convex curve such that:

$$sign\left(\frac{d^2 z_{rl}}{dy_{rl}^{\ 2}}\right) = sign\left(\frac{d^2 z_{rr}}{dy_{rr}^{\ 2}}\right) \equiv 1 . \tag{10}$$

In order to ensure that the optimized rail is also straight in the longitudinal direction, the following restrictions are made:

$$\max(z_{ref\,j} - z_{opt\,j}) \equiv C \tag{11}$$

where, C is a constant, j is the key cross sections number, z_{ref} is the vertical coordinate of the original rail profile, while z_{opt} is the vertical coordinate of the optimized rail profile.

The basic description of the profile design mathematical model can be expressed as follows:

$$\begin{cases} z_{rl}(y_w) = y_{wl}(y_w)\sin\phi_w(y_w) + z_{wl}(y_w)\cos\phi_w(y_w) + z_{w0} \\ z_{rr}(y_w) = y_{wr}(y_w)\sin\phi_w(y_w) + z_{wr}(y_w)\cos\phi_w(y_w) + z_{w0} \\ \dfrac{\mathrm{d}z_{rl}(y_w)}{\mathrm{d}y_{rl}(y_w)} = \tan\left(\operatorname{atan}\dfrac{\mathrm{d}z_{wl}(y_w)}{\mathrm{d}y_{wl}(y_w)} + \phi_w(y_w)\right) \\ \dfrac{\mathrm{d}z_{rr}(y_w)}{\mathrm{d}y_{rr}(y_w)} = \tan\left(\operatorname{atan}\dfrac{\mathrm{d}z_{wr}(y_w)}{\mathrm{d}y_{wr}(y_w)} + \phi_w(y_w)\right) \\ \tan\phi_w(y_w) = \dfrac{z_{wl}(y_w) - z_{wr}(y_w) - \dfrac{z_{rl}(y_w) - z_{rr}(y_w)}{\cos\phi_w(y_w)}}{y_{wr}(y_w) - y_{wl}(y_w)} \\ \Delta R(y_w) = z_{wl}(y_w) - z_{wr}(y_w) \end{cases} \tag{12}$$

$$s.t. \quad \begin{cases} z_{wl}(y_w) - z_{wr}(y_w) = \min\{z_{wl}(y_w) - z_{wr}(y_w)\big|_{y=yw}\} \\ sign\left(\dfrac{dz_{wl}}{dy_{wl}}\right) = sign\left(\dfrac{dz_{rl}}{dy_{rl}}\right) \equiv 1 \\ sign\left(\dfrac{dz_{wr}}{dy_{wr}}\right) = sign\left(\dfrac{dz_{rr}}{dy_{rr}}\right) \equiv -1 \\ sign\left(\dfrac{d^2 z_{rl}}{dy_{rl}^{\ 2}}\right) = sign\left(\dfrac{d^2 z_{rr}}{dy_{rr}^{\ 2}}\right) \equiv 1 \\ \max(z_{ref\,j} - z_{opt\,j}) \equiv C \end{cases} . \tag{13}$$

In fact, the design problem of rail profile in turnout area is a multi-objective optimization problem. If one wants to guarantee

the vehicle dynamic performance, like in this paper, the object function could be written as follows:

$$obj: f_1 = \min\left\{\frac{\int_{-y_{w\max}}^{y_{w\max}} (\left|\Delta R_{real}(y_w) - \Delta R_{opt}(y_w)\right|)\mathrm{d}y_w}{\int_{-y_{w\max}}^{y_{w\max}} \Delta R_{opt}(y_w)\mathrm{d}y_w} 100\%\right\} \quad (14)$$

where ΔR_{real} is the computed RRDF after the optimization, while ΔR_{opt} is the targeted optimization of RRDF.

We also treat wheel/rail contact point distribution as the auxiliary design target, the object function can be defined as follows:

$$obj: f_2 = \min\left(\sum_{i=1}^{k-1}\left|y_{rl}^{i+1}(y_w) - y_{rl}^{i}(y_w)\right| + \sum_{i=1}^{k-1}\left|y_{rr}^{i+1}(y_w) - y_{rr}^{i}(y_w)\right|\right) \quad (15)$$

where k is the number of contact points.

3. Equation solution and design procedure

In order to solve it in the form of numerical integration, the differential-algebraic equation (DAE) Eq. (12) must be expressed as ordinary differential equation (ODE) equations, both sides of the Eq. (12) must be derived from y_w at the same time. There are:

$$\begin{cases} \dfrac{dz_{rl}(y_w)}{dy_w} = \dfrac{dy_{wl}(y_w)}{dy_w}\cdot\phi_w(y_w) + \dfrac{d\phi_w(y_w)}{dy_w}\cdot y_{wl}(y_w) + \dfrac{dz_{wl}(y_w)}{dy_w} \\ \dfrac{dz_{rr}(y_w)}{dy_w} = \dfrac{dy_{wr}(y_w)}{dy_w}\cdot\phi_w(y_w) + \dfrac{d\phi_w(y_w)}{dy_w}\cdot y_{wr}(y_w) + \dfrac{dz_{wr}(y_w)}{dy_w} \\ \dfrac{\dfrac{dz_{rl}(y_w)}{dy_w}}{\dfrac{dy_{rl}(y_w)}{dy_w}} = \tan\left(\arctan\dfrac{dz_{wl}(y_w)}{dy_{wl}(y_w)} + \phi_w(y_w)\right) \\ \dfrac{\dfrac{dz_{rr}(y_w)}{dy_w}}{\dfrac{dy_{rr}(y_w)}{dy_w}} = \tan\left(\arctan\dfrac{dz_{wr}(y_w)}{dy_{wr}(y_w)} + \phi_w(y_w)\right) \\ \dfrac{d\phi_w(y_w)}{dy_w}\cdot\left(y_{rr}(y_w) - y_{rl}(y_w)\right) + \left(\dfrac{dy_{rr}(y_w)}{dy_w} - \dfrac{dy_{rl}(y_w)}{dy_w}\right)\cdot\phi_w(y_w) = \\ \dfrac{d\Delta R(y_w)}{dy_w} - \left(\dfrac{dz_{rl}(y_w)}{dy_w} - \dfrac{dz_{rr}(y_w)}{dy_w}\right) \\ \dfrac{d\Delta R(y_w)}{dy_w} = \dfrac{dz_{wl}(y_w)}{dy_{wl}(y_w)}\dfrac{dy_{wl}(y_w)}{dy_w} - \dfrac{dz_{wr}(y_w)}{dy_{wr}(y_w)}\dfrac{dy_{wr}(y_w)}{dy_w} \end{cases} . \quad (16)$$

In total, there are 11 unknown parameters in Eq. (16). In the switch area, the switch rail and the stock rail abut together to form a combined profile, and the non-working edge of the switch rail and the working edge of the stock rail form a special "concave" feature. Due to the special "concave" feature between the switch rail and stock rail of the turnout area, the designed profile still satisfies this feature. If the wheel-rail contact point on a certain side of the wheel is given [14, 15], the designed rail profile is a continuous curve, and the "concave" feature will not appear. The independent variable cannot be given casually. Therefore, it is necessary to give the parameters of the contact point on the rail with the switch rail side, that is, the rail transverse coordinates on the switch rail side should be given. Assuming that we know the ranges of (i) transverse abscissa of a rail on switch rail side (such as y_{rl}), (ii) lateral displacement of the wheelset (y_w), and (iii) objective function ($\Delta R(y_w)$). Moreover, wheel profile is known, that each of the two wheel profiles (y_{wl} , z_{wl}) and (y_{wr} , z_{wl}) have only one independent variable. So, they only have 2 independent variables (y_{wl} , y_{wr}).

$$\begin{cases} \dfrac{dz_{wl}(y_w)}{dy_w} = \dfrac{dz_{wl}(y_w)}{dy_{wl}(y_w)}\dfrac{dy_{wl}(y_w)}{dy_w} \\ \dfrac{dz_{wr}(y_w)}{dy_w} = \dfrac{dz_{wr}(y_w)}{dy_{wr}(y_w)}\dfrac{dy_{wr}(y_w)}{dy_w} \end{cases} . \quad (17)$$

These assumptions reduce the number of independent variables to six (i.e., 11-3-2 = 6). The Eq. (16) can be arranged as:

$$\begin{cases} \dfrac{dz_{rl}(y_w)}{dy_w} = \dfrac{dy_{wl}(y_w)}{dy_w}\cdot\phi_w(y_w) + \dfrac{d\phi_w(y_w)}{dy_w}\cdot y_{wl}(y_w) + \dfrac{dz_{wl}(y_w)}{dy_{wl}(y_w)}\dfrac{dy_{wl}(y_w)}{dy_w} \\ \dfrac{dz_{rr}(y_w)}{dy_w} = \dfrac{dy_{wr}(y_w)}{dy_w}\cdot\phi_w(y_w) + \dfrac{d\phi_w(y_w)}{dy_w}\cdot y_{wr}(y_w) + \dfrac{dz_{wr}(y_w)}{dy_{wr}(y_w)}\dfrac{dy_{wr}(y_w)}{dy_w} \\ \dfrac{\dfrac{dz_{rl}(y_w)}{dy_w}}{\dfrac{dy_{rl}(y_w)}{dy_w}} = \tan\left(\arctan\dfrac{dz_{wl}(y_w)}{dy_{wl}(y_w)} + \phi_w(y_w)\right) \\ \dfrac{\dfrac{dz_{rr}(y_w)}{dy_w}}{\dfrac{dy_{rr}(y_w)}{dy_w}} = \tan\left(\arctan\dfrac{dz_{wr}(y_w)}{dy_{wr}(y_w)} + \phi_w(y_w)\right) \\ \dfrac{d\phi_w(y_w)}{dy_w}\cdot\left(y_{rr}(y_w) - y_{rl}(y_w)\right) + \left(\dfrac{dy_{rr}(y_w)}{dy_w} - \dfrac{dy_{rl}(y_w)}{dy_w}\right)\cdot\phi_w(y_w) = \\ \dfrac{d\Delta R(y_w)}{dy_w} - \left(\dfrac{dz_{rl}(y_w)}{dy_w} - \dfrac{dz_{rr}(y_w)}{dy_w}\right) \\ \dfrac{d\Delta R(y_w)}{dy_w} = \dfrac{dz_{wl}(y_w)}{dy_{wl}(y_w)}\dfrac{dy_{wl}(y_w)}{dy_w} - \dfrac{dz_{wr}(y_w)}{dy_{wr}(y_w)}\dfrac{dy_{wr}(y_w)}{dy_w} \end{cases} . \quad (18)$$

The column vectors of all unknowns are separated into matrices in the form of:

$$A \times u = b \ . \quad (19)$$

Where,

$$A = \begin{bmatrix} 0 & 1 & 0 & -\left(\phi_w + \dfrac{dz_{wl}}{dy_{wl}}\right) & 0 & -y_{wl} \\ 0 & 0 & 1 & 0 & -\left(\phi_w + \dfrac{dz_{wr}}{dy_{wr}}\right) & -y_{wr} \\ -\tan\left(\arctan\dfrac{dz_{wl}}{dy_{wl}} + \phi_w\right) & 1 & 0 & 0 & 0 & 0 \\ 0 & 0 & 1 & 0 & 0 & 0 \\ 0 & 0 & 0 & \dfrac{dz_{wl}}{dy_{wl}} & -\dfrac{dz_{wr}}{dy_{wr}} & 0 \\ -\phi_w & 1 & -1 & 0 & 0 & y_{rr} - y_{rl} \end{bmatrix} \quad (20)$$

$$u=[\frac{dy_{rl}(y_w)}{dy_w}\quad\frac{dz_{rl}(y_w)}{dy_w}\quad\frac{dz_{rr}(y_w)}{dy_w}\quad\frac{dy_{wl}(y_w)}{dy_w}\quad\frac{dy_{wr}(y_w)}{dy_w}\quad\frac{d\phi_w(y_w)}{dy_w}]^T \tag{21}$$

$$b=[0\quad 0\quad 0\quad \tan\left(\arctan\frac{dz_{wr}}{dy_{wr}}+\phi_w\right)\cdot\frac{dy_{rl}(y_w)}{dy_w}\quad\frac{d\Delta R(y_w)}{dy_w}\quad\frac{d\Delta R(y_w)}{dy_w}-\frac{dy_{rr}(y_w)}{dy_w}\cdot\phi_w]^T \tag{22}$$

Solving Eq. (18) by Euler method,

$$\begin{cases} y_{k+1}=y_k+h\times f(x_k,y_k) \\ y_0=y(x_0) \end{cases}. \tag{23}$$

The profiles of wheel and rail to be optimized and basic wheel-rail contact parameters (rail gauge, the inner distance of the wheelset, axle load, wheel radius) are first given, which are used to obtain the rolling radius difference function curve in yw-△R coordinates. The curve is optimized, according to the vehicle operation requirements, and then used as the primary design objective function. Along with the expected wheel-rail contact distribution, the rail profile is inversely designed, i.e., put together with the reference rail profile to obtain the entire rail profile after the optimization. Verifications by such indicators as wheel-rail geometric contact, contact stress, and dynamics are performed for the newly designed rail profile. If not satisfactory, go back to modified rolling radius difference function, and the rail profile is redesigned until all requirements are met. The design flowchart is shown in Fig. 2. The optimized RRDF must satisfy the following criteria: (1) RRDF should be relatively small when the lateral displacement of wheelset is small, so that the vehicle stability on straight tracks is ensured; (2) RRDF should increase when the lateral movement of wheelset is larger, in order to improve the curving performance and reduce wear; (3) RRDF should be as smooth as possible.

4. Optimization examples

In order to verify the reliability of this paper, a group of turnouts (No. 12 single speed turnouts) in Yiwu Railway Station of Shanghai-Kunming Line of Shanghai Railway Administration was investigated and analyzed. When the turnout is in the straight through state, the train will shake violently and the contact band on the rail is too wide. According to the problems of this group of turnouts, an optimized grinding profile is proposed. After field grinding, the disease was eliminated.

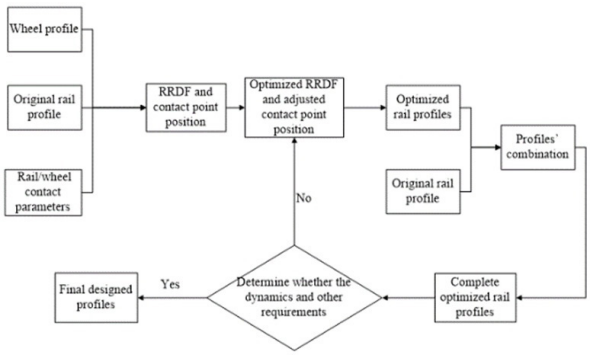

Fig. 2. Optimization design flow chart of rail in turnouts.

4.1 Measured wheel profiles

In order to more accurately analyze the wheel rail contact problem in the turnout area, the tracking measurement of passenger vehicles on Shanghai-Kunming railway was carried out, and 24 wheel profiles in different wear periods were measured, as shown in Fig. 3.

4.2 The switch problem

The rail profile of the switch area changes with the longitudinal distance. Therefore, it is difficult to represent the entire switch area with the one or two cross-section profiles. With the help of the rail profile measuring instrument, the profile measurement is carried out for some specific sections in the turnout switch area (a section named CQ is measured at the fifth sleeper in the front of the turnout; a section named CZ is measured at the first sleeper in front of the switch rail in the turnout, and then the sections with the width of the switch rail of 20 mm, 35 mm and 50 mm are measured respectively, named ZJ20, ZJ35 and ZJ50. At the 24th sleeper in the turnout, the section of a switch rail completely changed into stock rail was measured, named CH). There is a concave area between the switch rail and the stock rail, which is difficult to satisfy by the traditional continuous design method of rail profile in Fig. 4.

During the investigation and analysis of the switch area profile, it is found that the contact band of the rail in the switch area is excessively wide (which will cause abnormal shaking when the train passed through the turnout), the gauge angle side wear of switch rail was large, and the reduced value of turnout switch rail has not met the design requirements [28], see Fig. 5.

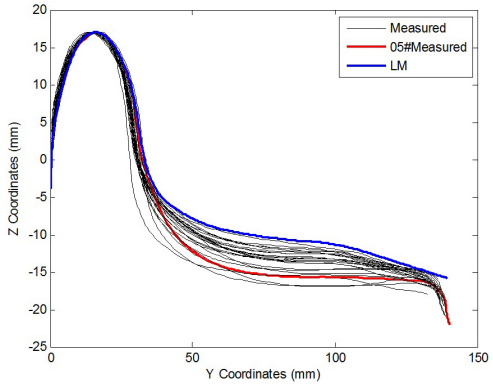

Fig. 3. 24 measured passenger vehicles wheel profiles together with a nominal LM profile.

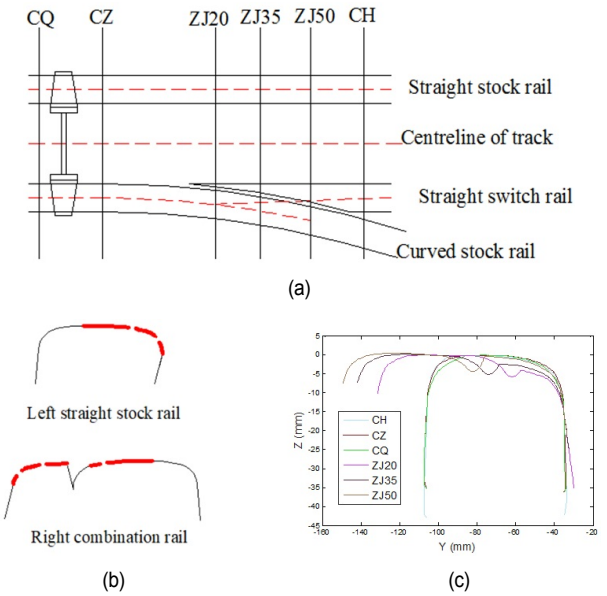

Fig. 4. Principle sketch of a switch area: (a) schematic; (b) optimize the region; (c) cross-sectional profiles.

Fig. 5. The rail profile in switch area.

4.3 Cross-sectional optimization

In the process of optimization design, the wheel tread selected 05# measurement profile, and optimized design for the five cross-sections CQ, ZJ20, ZJ35, ZJ50 and CH. Assuming that the given wheel radius is 420 mm, the inner distance of the wheelset is 1353 mm, the gauge is 1435 mm, and the gauge measurement point is 16 mm from the top of the rail. ZJ50 section is taken as an example to illustrate.

When the width of switch rail is 50 mm (ZJ50 cross-section), The wheel-rail geometric contact characteristics obtained with disregard of the wheelset yaw angle effect are shown in Fig. 6: the wheel-rail contact points concentration and partial jump are observed in the stock rail.

The comparative analysis of Fig. 6 reveals the apparent jump phenomenon for the contact point when the lateral displacement is within [-1 mm, 0 mm] and [2 mm, 3 mm] ranges, which causes the rail vehicle to encounter multiple points when it passes the straight turnout. This will result in uneven wear and a more significant impact, which eventually leads to the reduction of the rail service life.

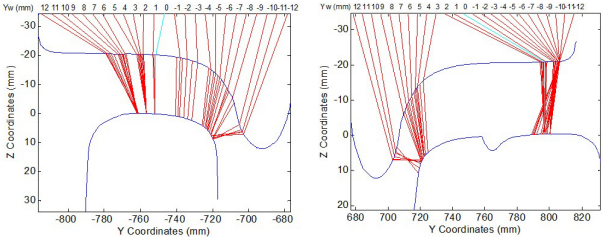

Fig. 6. The wheel-rail contact before optimization.

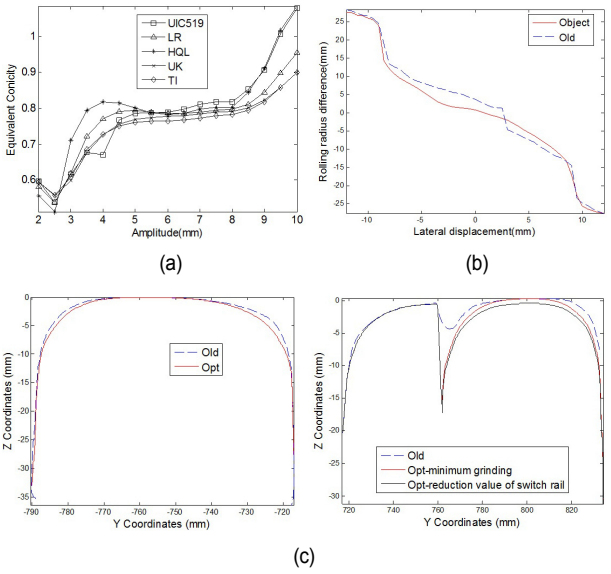

Fig. 7. (a) Equivalent conicity; (b) old and object RRD curves; (c) comparison of rail profiles before and after optimization.

As shown in Fig. 7(a), the equivalent conicity exceeds 0.5, which seriously endangers the stability and safety of the train.

To ensure the dynamic performance of the vehicle when crossing the turnout and the mechanical requirements related to wheel rail contact, RRDF needs to meet the following characteristics:

1) When the wheelset lateral displacement is very small, the RRDF value is very small, to have a small equivalent taper and ensure the stability of the vehicle on a straight track.

2) When the lateral displacement of wheelset is ±3 mm ~ ±8 mm, the RRDF curve shall be as wide and smooth as possible to reduce the jumping phenomenon of wheel rail contact point. At the same time, the RRDF value is large to ensure that the vehicle can pass through the curve smoothly.

3) When the lateral displacement of wheelset is ±8 mm ~ ±10 mm, the RRDF value shall be as large as possible to ensure the derailment safety.

In order to reduce the equivalent conicity, jump of the wheel-

rail contact point and width of the contact band on the rail, the optimization object is shown in Fig. 7(b).

The corresponding optimized rail profile is displayed in Fig. 7(c). In order to ensure that the reduction value of the switch rail can meet the requirement of 0 mm at this section, the right stock rail needs to be shifted downward properly to meet the requirements of the reduced value of the switch rail (In the actual rail grinding operation, it is necessary to pad the switch rail to a suitable height, as shown in Fig. 7(c), the pad height of this cross section is about 0.8 mm. Usually, adjusting the thickness of the foot pad under the basic rail is used to reduce the value of the switch rail to meet the design standards).

The wheel-rail contact was re-calculated and analyzed for the optimized profiles, see Fig. 8. Optimized wheel rail contact points are more evenly distributed, and the jumping phenomenon of wheel rail contact points is reduced. The wheel rail contact points of the right rail completely jump from the stock rail to the switch rail, and the contact band is narrow when the wheelset lateral displacement is -5 mm to 5 mm.

Fig. 9(a) shows that after the curved turnout optimization the RRDF curve agrees very well with the targeted curve (object RRD), with a maximum error of 4.19 % and an average error of 2.11 %. Moreover, a relatively large error in the lateral displacement mainly occurs the contact point at the wheel flange. As shown in Fig. 9(b), the equivalent conicity is less than 0.18, which fully satisfy requirements of the straight design.

4.4 Longitudinal profile optimization

In order to simplify this paper, we only give the design process when the tip width of the switch rail is 50 mm (ZJ50 cross section). According to the same design method, we can design other key sections (such as the CQ, ZJ20, ZJ35, CH), as shown in Fig. 10. Although the variable section profile of a group of turnouts can be divided into several key sections for optimal design, these key sections are not completely independent in the longitudinal direction. It is also necessary to ensure that the wheel rail contact light belt is as smooth as possible in the longitudinal direction, and control the width of the contact light belt between 20-30 mm, which is conducive to the stability of vehicle operation and wheel rail wear. Therefore, another constraint function has to be given:

$$obj: f_3 = \min\left(\max\left|y_{wl}(y_w = m) - y_{wl}(y_w = n)\right| + \max\left|y_{wr}(y_w = m) - y_{wr}(y_w = n)\right|\right) \quad (24)$$

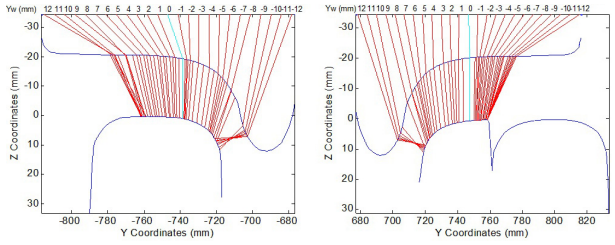

Fig. 8. The wheel-rail contact after optimization.

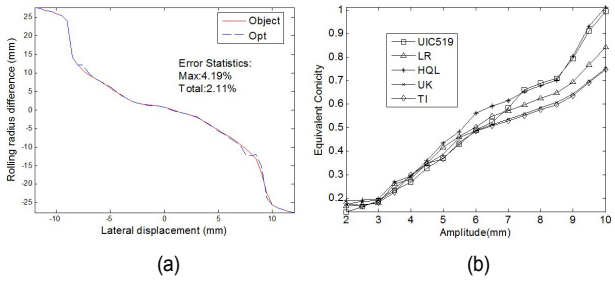

(a) (b)

Fig. 9. (a) Error statistics of the optimized RRD; (b) equivalent conicity.

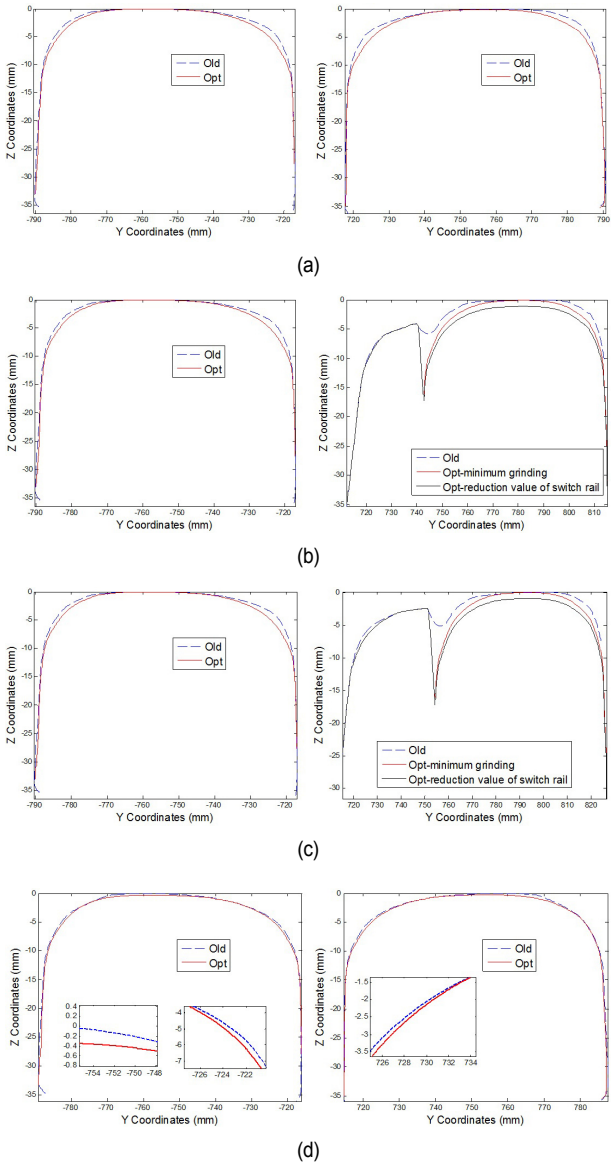

(a) (b) (c) (d)

Fig. 10. Before and after optimization of CQ: (a) ZJ20; (b) ZJ35; (c) CH; (d) cross-section rail profiles.

where m is the minimum lateral displacement of wheelset, n is the maximum lateral displacement of wheelset.

It takes about 30 seconds to design a single cross-section, and the design parameters need to be modified several times in order to ensure that the results of the optimization design meet the design requirements, which is more efficient than other optimization methods.

4.5 Dynamic verification

With the help of MATLAB and Simulink platform, the dynamic model of the vehicle (Chinese PW220-K [24]) passing through the turnout to verify the dynamic performance before and after optimization. Using the 05# wheel tread, a rail vehicle passage of a CN60-350-1:12 single straight turnout was simulated. The vehicle speed passing such turnout should not exceed 120 km/h [28].

The matrix assembly method is used to construct the vehicle dynamic model. It can be described as:

$$[M]\ddot{x}+[C]\dot{x}+[K]x=F \tag{25}$$

where $[M]$, $[C]$, and $[K]$ are system mass, damping, and stiffness matrix, respectively. F is the generalized force vector. x is the response vector.

In the wheel-rail contact model, the SHEN-Hedrick theory is used to solve the tangential contact problem, First, it is calculated according to Kalker's linear creep theory, and then the SHEN-Hedrick method is used to correct the creep saturation.

The simulation results include the leading wheelset lateral displacement, the wear index, the vertical and lateral wheel-rail contact force for the leading wheelset at the side of the switch rail are also investigated, as shown in Fig. 11. When the vehicle passes through the optimized turnout area, the dynamic performance is better. The maximum lateral displacement of wheelset is 5.3 mm for the nominal profile and is 3.2 mm for the optimized profile. The maximum wear index decreased from 1396 before optimization to 1348. After optimization, the vertical force, wheel-rail lateral force was reduced.

From the dynamic simulation, before optimization, the vehicle will produce severe impact when passing through the turnout, and many dynamic indexes will fluctuate greatly. After optimization, although the vehicle will also have impact when passing through the turnout, the impact effect is small because the optimized rail profile is smoother along the longitudinal direction.

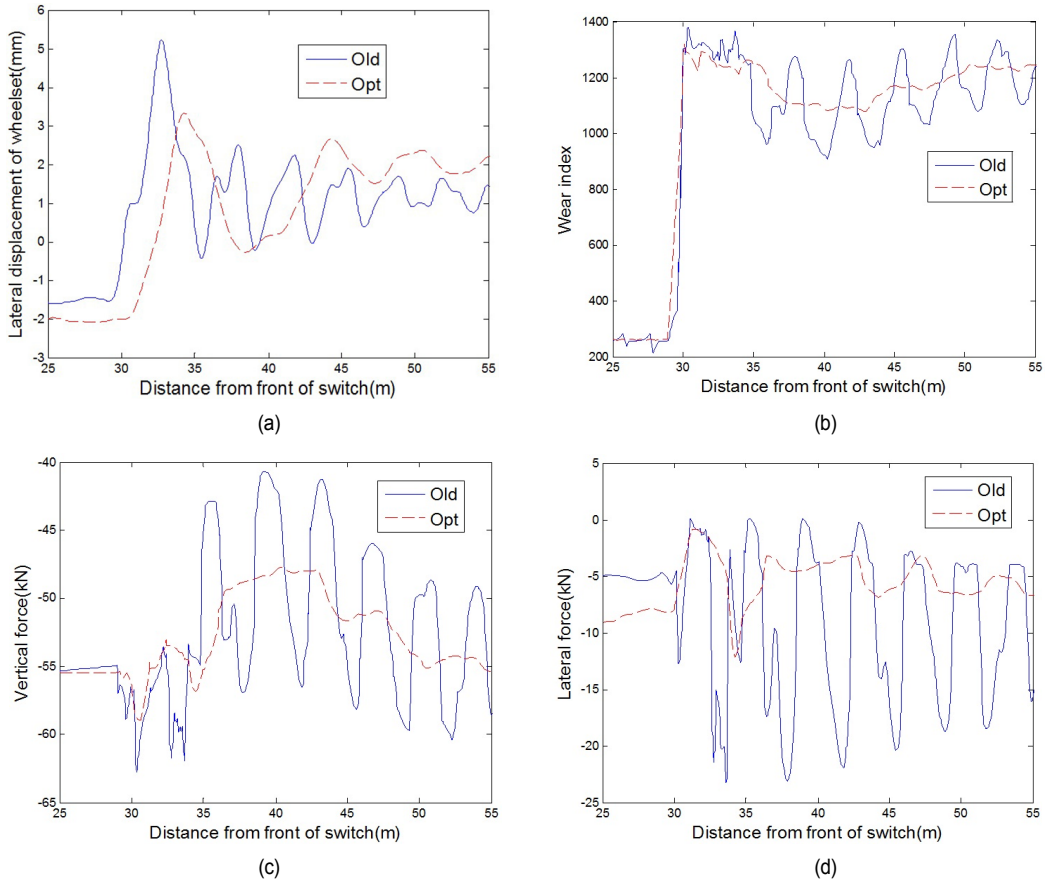

Fig. 11. The comparison of dynamic interaction: (a) lateral displacement of wheelset; (b) wear index; (c) vertical force; (d) lateral force.

Table 1. The equivalent conicity at stock rail.

Wheel number	Equivalent conicity				Evaluate
	Before (CQ)	Before (CZ)	Before (CH)	Optimization	
001	0.16	0.31	0.25	0.11	Good
002	0.35	0.65	0.67	0.2	Good
003	0.44	0.7	0.75	0.22	Good
004	0.17	0.15	0.25	0.1	Good
005	0.55	1.1	1.05	0.29	Good
006	0.55	0.36	0.37	0.53	Slightly poor
007	0.3	0.61	0.65	0.45	Slightly poor
008	0.2	0.16	0.28	0.14	Good
009	0.18	0.44	0.35	0.1	Good
010	0.3	0.42	0.5	0.2	Good
011	0.6	0.92	0.95	0.45	Good
012	0.41	0.42	0.45	0.37	Good
013	0.12	0.11	0.13	0.09	Good
014	0.11	0.09	0.1	0.09	Good
015	0.18	0.34	0.22	0.18	Good
016	0.32	0.52	0.6	0.2	Good
017	0.46	0.53	0.63	0.43	Good
018	0.39	0.68	0.6	0.22	Good
019	0.6	0.74	0.75	0.33	Good
020	0.17	0.13	0.16	0.11	Good
021	0.25	0.4	0.43	0.19	Good
022	0.28	0.51	0.47	0.18	Good
023	0.23	0.37	0.36	0.13	Good
024	0.3	0.51	0.56	0.16	Good

4.6 A series of wheel verification

The above sections only aim at the 5# wheel as the design template to optimize the design of turnout. From the optimization results, the optimization effect can well meet the design requirements. But there are a lot of wheels measured on the line. Can the optimized profile meet the rest of the wheels? Therefore, it is necessary to calibrate the rest of the wheels, and this group of turnouts is mainly in the straight through state. In order to reduce the lengthy of the paper, only the equivalent conicity of each wheel and rail at each section is verified and analyzed.

The validity of CQ, CZ and CH cross-sections is tested, as shown in Table 1. After optimization, most of the equivalent conicity are decreased. If the evaluation is good, it means that at this cross-section, the equivalent conicity of this wheelset is lower than before optimization; if the evaluation is slightly poor, it means that at this cross-section, the equivalent conicity of the wheelset is increased than before optimization. There are 3 rail cross-sections and 24 wheel treads (3 wheel tread verification results are slightly poor), so the pass rate is [1-4/(24*3)] = 94.44 %, indicating that the optimization results satisfy the requirements of the series of the wheels.

The validity of ZJ20, ZJ35 and ZJ50 cross-sections is tested, as shown in Table 2. After optimization, most of the equivalent conicity are decreased. There are 3 rail cross-sections and 24 wheel treads (4 wheel tread verification results are slightly poor), so the pass rate is [1-4/(24*3)] = 94.44 %, indicating that the optimization results satisfy the requirements of the series of the wheels.

This switch area cross-profile design has proven that the proposed method is effective and efficient. Plenty of choice of free variables also reflects the flexibility of the method. Practical implementation has been carried out at several grinding sites in China.

5. Conclusions

The results obtained make it possible to draw the following conclusions:

We introduced an inverse rail profile design method for rails in the switch area of railway turnouts, which allows one to improve the wheel-rail contact and dynamic performance of rail vehicles during their passage of turnouts. The rolling radius difference function (RRDF), which refers to the left and right rolling radius difference versus wheelset lateral movement, is used as the primary optimization criterion. The method application is shown to reduce include the lateral displacement of wheelset, the vertical and lateral wheel-rail contact force and the wear index at the side of the switch rail. The method makes the turnouts smoother in the longitudinal direction, and reduces the wheel-rail dynamic force when the wheel-rail contact point jumps from the stock rail to the switch rail. Besides, it makes the geometric contact between wheel and rail more uniform, which helps to reduce the contact stress, wear and rolling contact fatigue between rails and wheels. All these improvements can prolong the rail service life.

This method can not only develop the grinding profiles for rails in turnouts but also ensure that the maximum grinding amount in each cross section of the designed profile is consistent. This avoids the occurrence of wavy lines and satisfy the decline requirements of the switch rail, which makes the proposed design method quite instrumental in designing new profiles for rails in turnouts. The application of rail profile design in turnout area has been carried out in China, and good results have been achieved. This technology will be further promoted in the future.

This paper considers neither the compatibility of optimized rail profiles with other types of wheels nor cases of multi-point contact in the turnout area. These topics will be further investigated in the future work.

Acknowledgments

This work is partly supported by the National Natural Science Foundation of China (No. 62103285: Research on an adaptive

pedestrian navigation method in unfamiliar environment based on cooperative probabilistic map by the MEME IMU array), China, the project of Shanghai Science and Technology Commission Local Capacity Building (No.22YF1447600: Study on variable cross section profile optimization of high-speed turnout oriented to wear control; No.20090503100: Research on Key Technologies of rail transit intelligent operation and maintenance, No.20511103100: Development and demonstration application of spatial panoramic data acquisition equipment for complex environment of super large city), China, the Talent Introduction Scientific Research Foundation of Shanghai Institute of Technology (No.10120K216061-A06: Research on mechanism and improvement measures of abnormal lateral low frequency swaying of rail vehicles), China.

Nomenclature

RRDF : Rolling radius difference function
RRF : Rolling radius difference
RCF : Rolling contact fatigue
CAF : Contact angle function
C : Constant
DAE : Differential algebraic equation
ODE : Ordinary differential equation
LM : A Chinese wheel profile name

References

[1] N. Burgelman, Z. Li and R. Dollevoet, A new rolling contact method applied to conformal contact and the train-turnout interaction, *Wear*, 321 (2014) 94-105.
[2] J. M. Xu, P. Wang, L. Wang and R. Chen, Effects of profile wear on the wheel-rail contact conditions and dynamic interaction of vehicle and turnout, *Advances in Mechanical Engineering*, 8 (1) (2016) 1-14.
[3] R. Skrypnyk, U. Ossberger, B. A. Pålsson, M. Ekh and J. C. O. Nielsen, Long-term rail profile damage in a railway crossing: Field measurements and numerical simulations, *Wear*, 472-473 (2021) 203331.
[4] E. E. Magel and J. Kalousek, The application of contact mechanics to rail profile design and rail grinding, *Wear*, 253 (1) (2002) 308-316.
[5] S. Zakharov, I. Goryacheva and V. Bogdanov, Problems with wheel and rail profiles selection and optimization, *Wear*, 265 (9-10) (2008) 1266-1272.
[6] I. Y. Shevtsov, V. L. Markine and C. Esveld, Optimal design of wheel profile for railway vehicles, *Wear*, 258 (7) (2005) 1022-1030.
[7] V. L. Markine, I. Y. Shevtsovand and C. Esveld, An inverse shape design method for railway wheel profiles, *Struct Multidisc Optim*, 33 (2007) 243-253.
[8] G. Shen and X. Zhong, A design method for wheel profiles according to the rolling radius difference function, *Proceedings of the Institution of Mechanical Engineers Part F Journal of Rail and Rapid Transit*, 225 (5) (2011) 457-462.
[9] D. B. Cui, L. Li and X. S. Jin, Optimal design of wheel profiles based on weighed wheel/rail gap, *Wear*, 271 (2001) 218-226.
[10] M. Ignesti, A. Innocenti and L. Marini, Wheel profile optimization on railway vehicles from the wear viewpoint, *International Journal of Non-Linear Mechanics*, 53 (2013) 41-45.
[11] J. Santamaria, J. Herreros, E. G. Vadillo and N. Correa, Design of an optimised wheel profile for rail vehicles operating on two-track gauges, *Vehicle System Dynamics*, 51 (1) (2013) 54-73.
[12] H. Choi, D. Lee, C. Y. Song and J. Lee, Optimization of rail profile to reduce wear on curved track, *International Journal of Precision Engineering and Manufacturing*, 14 (4) (2013) 619-625.
[13] J. Wang, S. Chen, X. Li and Y. Wu, Optimal rail profile design for a curved segment of a heavy haul railway using a response surface approach, *Proceedings of the Institution of Mechanical Engineers Part F Journal of Rail and Rapid Transit*, 230 (6) (2016).
[14] X. Mao and G. Shen, An inverse design method for rail grinding profiles, *Vehicle System Dynamics*, 55 (7) (2017) 1029-1044.
[15] X. Mao and G. Shen, A design method for rail profiles based on the geometric characteristics of wheel-rail contact, *Proceedings of the Institution of Mechanical Engineers Part F Journal of Rail and Rapid Transit*, 232 (5) (2018) 1255-1265.
[16] W. M. Zhai, J. M. Gao and P. F. Liu, Reducing rail side wear on heavy-haul railway curves based on wheel-rail dynamic interaction, *Vehicle System Dynamics*, 52 (2014) 440-454.
[17] D. Nicklisch, E. Kassa, J. Nielsen, M. Ekh and S. Iwnicki, Geometry and stiffness optimization for switches and crossings, and simulation of material degradation, *Proceedings of the Institution of Mechanical Engineers Part F Journal of Rail and Rapid Transit*, 224 (4) (2010) 279-292.
[18] P. Wang, X. Ma, J. Wang, J. Xu and R. Chen, Optimization of rail profiles to improve vehicle running stability in switch panel of high-speed railway turnouts, *Mathematical Problems in Engineering*, 2017 (2017) 2856030.
[19] B. Pålsson, Optimisation of railway crossing geometry considering a representative set of wheel profiles, *Vehicle System Dynamics*, 53 (2) (2015) 274-301.
[20] B. Pålsson, Design optimisation of switch rails in railway turnouts, *Vehicle System Dynamics*, 51 (10) (2013) 1619-1639.
[21] M. R. Bugarín, J. M. García and D. D. Villegas, Improvements in railway switches, *Proceedings of the Institution of Mechanical Engineers Part F Journal of Rail and Rapid Transit*, 216 (4) (2002) 275-286.
[22] J. C. O. Nielsen, B. A. Palsson and P. T. Torstensson, Switch panel design based on simulation of accumulated rail damage in a railway turnout, *Wear*, 366 (2016) 241-248.
[23] J. R. Oswald, Turnout geometry optimization with dynamic simulation of track and vehicle, *AREMA Proceedings of the 2000 Annual Conference*, American Railway Engineering and Maintenance of Way Association, Dallas, TX (2000) 297-302.
[24] D. L. Chen, G. Shen, X. Mao and B. C. Chen, A design method for rail profiles in switch panel of turnout based on the contact stress analysis, *Shock and Vibration*, 2020 (2020) 8575498.
[25] C. Wan, V. L. Markine and I. Y. Shevtsov, Improvement of

vehicle-turnout interaction by optimising the shape of crossing nose, *Vehicle System Dynamics*, 52 (11) (2014) 1517-1540.
[26] Z. S. Ren, *Wheel/Rail Multi-Point Contacts and Vehicle-Turnout System Dynamic Interactions*, Beijing: Science Press (2014) (in Chinese).
[27] G. Shen, *Railway Vehicle System Dynamic*, Beijing: China Railway Publishing House (2014) (in Chinese).
[28] The Committee of Routine Turnout Main Parameters Handbook, *Routine Turnout Main Parameters Handbook*, China Railway Publishing House, Beijing, China (2007) (in Chinese).

Dilai Chen is s a lecturer at the School of Railway Transportation, Shanghai Institute of Technology. He received his Ph.D. in Vehicle Engineering from Tongji University. His research interests include vehicle system dynamics and wheel-rail profile design.